

Selective and Scalable Control of Spin Quantum Memories in a Photonic Circuit

D. Andrew Golter,* Genevieve Clark,* Tareq El Dandachi, Stefan Krastanov, Andrew J. Leenheer, Noel H. Wan, Hamza Raniwala, Matthew Zimmermann, Mark Dong, Kevin C. Chen, Linsen Li, Matt Eichenfield,* Gerald Gilbert,* and Dirk Englund*



Cite This: *Nano Lett.* 2023, 23, 7852–7858



Read Online

ACCESS |

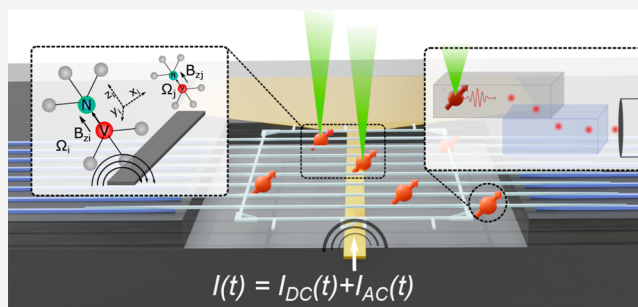
Metrics & More

Article Recommendations

Supporting Information

ABSTRACT: A central goal in many quantum information processing applications is a network of quantum memories that can be entangled with each other while being individually controlled and measured with high fidelity. This goal has motivated the development of programmable photonic integrated circuits (PICs) with integrated spin quantum memories using diamond color center spin-photon interfaces. However, this approach introduces a challenge into the microwave control of individual spins within closely packed registers. Here, we present a quantum memory-integrated photonics platform capable of (i) the integration of multiple diamond color center spins into a cryogenically compatible, high-speed programmable PIC platform, (ii) selective manipulation of individual spin qubits addressed via tunable magnetic field gradients, and (iii) simultaneous control of qubits using numerically optimized microwave pulse shaping. The combination of localized optical control, enabled by the PIC platform, together with selective spin manipulation opens the path to scalable quantum networks on intrachip and interchip platforms.

KEYWORDS: diamond color center, integrated photonics, spin control, optimal control, quantum information



A network of entangled quantum memories is an essential component of many emerging quantum technologies. These memories must be individually controllable with high fidelity, have long coherence times, and be implemented in a scalable way. Recently proposed blueprints for general-purpose quantum information processing call for solid-state spin-based quantum memories connected by switchable photonic links.^{1–3} These blueprints have motivated the development of cryogenic photonic integrated circuit (PIC) platforms^{4,5} and hybrid integration with diamond color centers.^{6,7}

As a first step toward integrating spin memories^{8–12} into such scalable PIC-based architectures, high-performance single-channel devices were demonstrated with single color centers coupled to photonic waveguides.^{13–18} Recently multichannel diamond waveguide arrays supporting multiple stable color centers were successfully incorporated into a photonic integrated circuit using a high-yield, scalable process.^{6,17} To realize the potential of these color-center-based devices for large-scale quantum information processing, this scalable photonic integration needs to be accompanied by scalable electron spin control. Microwave control of color center spins enables state manipulation,^{19,20} entanglement generation,^{21–24} and state transfer with long-lived nuclear memories.^{25–29}

Here we demonstrate microwave control over many spins integrated into a scalable piezo-optomechanical photonics platform and explore methods of scaling this control.

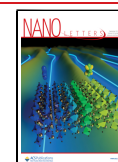
First we describe on-chip spin control of diamond nitrogen-vacancy (NV) centers integrated into our PICs, fabricated in a wafer-scale, 200 mm CMOS-foundry process.^{4,5,30,31} Our device structure, shown in Figure 1a, couples NV fluorescence to on-chip silicon nitride (SiN) waveguides and an edge-coupled optical fiber, enabling scalable and efficient optically networked state readout. A microwave transmission line beneath the color centers delivers a time-varying current, with a corresponding magnetic field, that allows for spin-state control.

Scalability requires that individual, high-fidelity state control must be applied simultaneously to many optically networked spin qubits. However, maintaining separate microwave control channels for each qubit would dramatically increase the

Received: April 21, 2023

Revised: July 7, 2023

Published: August 29, 2023



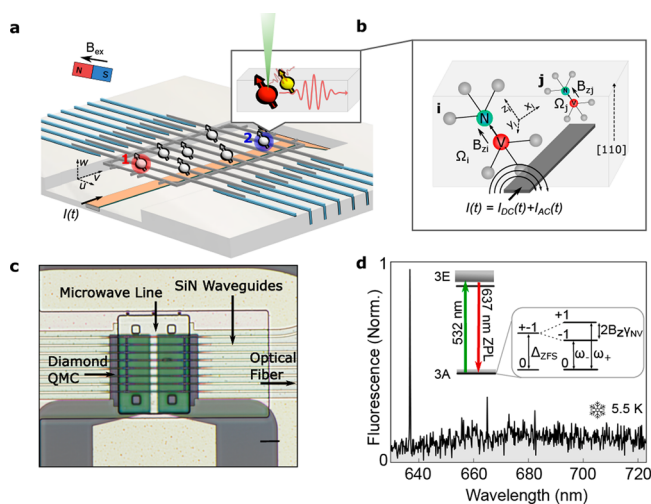


Figure 1. (a) Device structure showing spins in a QMC heterogeneously integrated into a PIC. A free-space laser excites NV centers at a particular location in the diamond waveguide, while NV fluorescence couples to the diamond waveguide mode. In the diamond sample used here, multiple NVs were present at each excitation spot. (b) A current $I(t)$ supplied through the microwave line is used to manipulate NV spin qubits in the QMC. (c) Optical microscope image of the PIC showing an integrated wire for the delivery of microwaves below the diamond QMC. The scale bar is $6 \mu\text{m}$. (d) Low-temperature photoluminescence (PL) spectrum of NV centers in the QMC. The inset shows the energy level diagram for NV centers subject to magnetic field B_z .

hardware requirements. Time-frequency multiplexed microwave control offers an alternative in which many spin qubits can be controlled through a single microwave channel. In a multiplexed scheme, scalability requires selectivity in control,^{32–35} i.e., it should be possible to apply a single-qubit gate on one spin while keeping the level of cross-talk with other spins low. Upon application of a single-qubit rotation by operator U_i on a selected spin i , the error on another spin j is given by

$$\epsilon_j = 1 - |\langle j_{0,1} | U_i | j_{0,1} \rangle|^2 \quad (1)$$

where U_j is the corresponding time propagator for spin j and the notation indicates that the expectation value is calculated in the ground or excited state.

In the rotating frame of a microwave control field with angular frequency ω_{mw} , Rabi frequency $\Omega(t)$, and phase $\varphi(t)$, the Hamiltonian describing the interaction with spin i (which we model as a two-level system) is

$$H_i = \frac{1}{2} \hbar (\Delta_i \sigma_z + \Omega_i(t) \{ \cos[\varphi_i(t)] \sigma_x + \sin[\varphi_i(t)] \sigma_y \}) \quad (2)$$

where Ω_i and Δ_i must be real and σ_x and σ_y are Pauli matrices. $\Delta_i = \omega_{+,i} - \omega_{\text{mw}}$ is the detuning from spin transition frequency $\omega_{+,i}$, which in a static magnetic field $\vec{B}(\vec{r}_i)$, with small off-axis components, is approximately

$$\omega_{+,i} = D_{\text{zfs}} + \gamma_{\text{NV}} B_{z,i} \quad (3)$$

where D_{zfs} is the zero-field splitting, $B_{z,i} = \hat{z} \cdot \vec{B}(\vec{r}_i)$ is the magnetic field component along the dipole axis (see Figure 1b), and γ_{NV} is the NV gyromagnetic ratio.

Applying a σ_x rotation on spin i involves setting $\Delta_i = 0$, $\Omega_i(t) = \Omega_{\text{p}}$, and $\varphi_i(t) = 0$ for a time $T \ll T_2$, where $T\Omega_i = \pi$ and T_2 is the spin coherence time. During this process, spin j undergoes

evolution from state $|j_0\rangle \rightarrow |j_T\rangle = U_j |j_0\rangle$. If $\Omega_j/\Delta_j \ll 1$, the state error is bounded from above by $\epsilon_j = (\Omega_j/\Delta_j)^2$ (see Supporting Information 1). This means that a low level of cross-talk is possible if the spin transitions are well separated compared to Rabi frequency Ω_j . To achieve the $\Omega_j/\Delta_j \ll 1$ requirement for “selective frequency addressing”, we use a magnetic field gradient, generated on chip and localized to the quantum memory register, to produce a position-dependent shift in $\omega_{+,i}$. Using this method, we demonstrate frequency-resolved control over spins at several different locations within a single waveguide.

However, if spectral spacing Δ_j is too small or we want to drive the dynamics quickly, yielding a large Ω_j , selective spin control is also possible by temporal modulation of $\Omega(t)$ and $\varphi(t)$. Under this scheme, all spins will exhibit non-negligible evolution under the application of the control field, but they will follow different trajectories. This opens up the possibility that, through the careful shaping of $\Omega(t)$ and $\varphi(t)$ via the tools of optimal control theory, the spins can be guided to a desired end state, effectively executing selective control even when the conditions for full frequency resolution are not met. We conclude by considering, theoretically and experimentally, this simultaneous control using optimally shaped microwave pulses.

We performed experiments on naturally occurring NV^- centers in an eight-waveguide single-crystal diamond “quantum micro-chiplet” (QMC) integrated over a microwave transmission line on a silicon nitride (SiN) PIC, as shown in panels a and c of Figure 1. The diamond QMC waveguides (see ref 12 for fabrication) and SiN waveguides on the PIC (see ref 17) couple optically via inverse tapering, as detailed previously.¹⁷ Details of the waveguide dimensions and coupling efficiency are described in Supporting Information 2. Optical excitation of the color centers occurs through free space perpendicular to the chip, while fluorescence is collected from the SiN waveguides into an edge-coupled optical fiber. With the excitation laser positioned at location 1 in Figure 1a, we observe a clear NV zero-phonon line when collecting fluorescence through the PIC at 5 K, as shown in Figure 1d. All of the other measurements were performed at room temperature.

Figure 1b illustrates our approach to spin control of NV centers in a QMC using the microwave line. A current with both an ac component and a dc component, $I(t) = I_{\text{dc}} + I_{\text{ac}}(t) \sin(\omega_{\text{mw}}t + \phi_{\text{mw}})$, where $I_{\text{ac}}(t)$ varies slowly compared with ω_{mw} is applied through the microwave line creating a spatially dependent dc magnetic field, $\vec{B}_{\text{dc}}(\vec{r})$, and a time and spatially dependent ac magnetic field, $\vec{B}_{\text{ac}}(t, \vec{r}) \sin(\omega_{\text{mw}}t + \phi_{\text{mw}})$, with $|\vec{B}_{\text{dc}}| \propto I_{\text{dc}}$ and $|\vec{B}_{\text{ac}}| \propto I_{\text{ac}}$. In addition, an external magnet provides a constant magnetic field, \vec{B}_{ext} , that is spatially invariant at the length scale of the QMC. The spin $|\pm 1\rangle$ sublevels for NV i at position \vec{r}_i undergo a Zeeman shift (see eq 3) yielding spin transitions at

$$\omega_{\pm,i} = D_{\text{zfs}} \pm \gamma_{\text{NV}} [B_{\text{ext},z} + B_{\text{dc},z}(\vec{r}_i)] \quad (4)$$

as shown in the inset of Figure 1. When $\omega_{\text{mw}} = \omega_{\pm,i}$ the spin transition is driven at the Rabi frequency, $\Omega_i(t) = \frac{1}{\sqrt{2}} \gamma_{\text{NV}} B_{\text{ac},xy}(t, \vec{r}_i)$, where $B_{\text{ac},xy}$ is the component of the ac magnetic field perpendicular to the dipole axis.

We begin by setting I_{dc} to 0. Figure 2a shows optically detected magnetic resonance (ODMR) when optically pumping location 2 is indicated in Figure 1a. We observe three resonance pairs, indicating at least three NV centers at

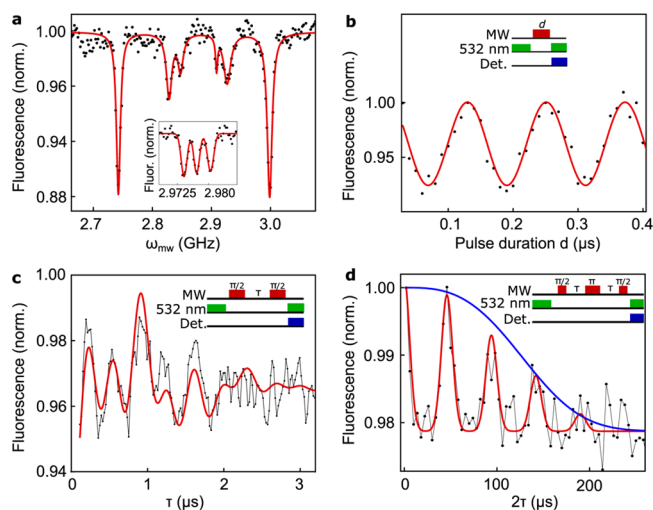


Figure 2. (a) ODMR spectrum measured in a static uniform dc magnetic field under continuous microwave excitation. The inset that shows the ODMR spectrum measured under low excitation power reveals triplet hyperfine structure due to coupling to the nitrogen nuclear spin. (b) Spin-dependent fluorescence as a function of the microwave pulse duration shows Rabi oscillations when the microwave field is resonant with a particular spin transition. (c) Ramsey fringes reveal a T_2^* of 1.7 μs . The red line is a fit using three exponentially decaying sine waves with frequencies given by the detuning for each of the hyperfine states. (d) A Hahn echo sequence reveals a T_2 of 150 μs . The echo signal collapses and is revived at the frequency of the Larmor precession of nearby ^{13}C nuclear spins.

this location in the QMC, with different orientations relative to \vec{B}_{ext} . The inset shows the spin-triplet hyperfine structure of the prevalent ^{14}NV isotope. With the microwave field tuned to one of the resonances, $\omega_{\text{mw}}/2\pi = 3.00$ GHz, measurements following the pulse sequence shown in the inset of Figure 2b produce Rabi oscillations at $\Omega_i/2\pi = 7.5$ MHz. We next apply this spin control to Ramsey fringe (Figure 2c) and Hahn echo (Figure 2d) measurements, yielding coherence times for this spin memory of $T_2^* = 1.7$ μs and $T_2 = 150 \pm 5$ μs , typical for NV spins in diamond nanostructures.^{34–38} For the remainder of the measurements in this paper, we consider only the NV subpopulation corresponding to the feature at 3.00 GHz in Figure 2a and set \hat{z} along the corresponding dipole axis.

To demonstrate selective frequency addressing, we now set $I_{\text{dc}} \neq 0$, giving $\omega_{\pm,i}$ a spatial dependence (eq 4). Assuming all spins are initialized to $|0\rangle$, the cross-talk error on spin j under a π -pulse on spin i is $\epsilon_j = 1 - \langle 0|U_i|0\rangle^2$. Figure 3a plots the simulated ϵ_j for a spin at different spatial locations relative to the microwave line at $u = 0$, when a π -pulse, with $\Omega_i/2\pi = 10$ MHz chosen to match the experiment, is applied to a target spin i located at $u = 1.5$ μm . The cases in which $I_{\text{dc}} = 0$ and 150 mA are compared. We determine the spatial dependence of \vec{B}_{dc} and \vec{B}_{ac} from finite-element simulations based on the current in the microwave line. We then calculate $B_{\text{dc},z}$ and $B_{\text{ac},xy}$ for an NV dipole axis with $\theta_w = 54.7^\circ$ for NVs in a $[100]$ -oriented diamond and with $\theta_u = 41.0^\circ$ set to be consistent with our experimental data for the subpopulation of NV centers considered in this work. When $I_{\text{dc}} = 150$ mA, ϵ_j is expected to decrease significantly within a few micrometers of the target spin, while when $I_{\text{dc}} = 0$ mA, ϵ_j remains large at locations many micrometers from the target qubit [Figure 3b(i)]. The spatially varying Zeeman shift [Figure 3b(ii)] has led to a position-

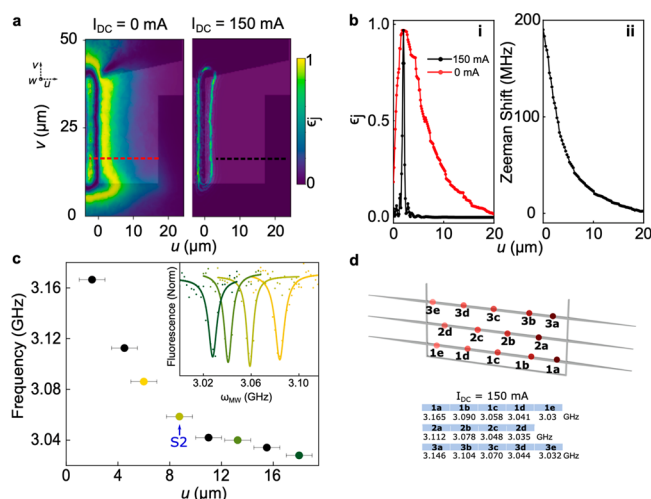


Figure 3. (a) Simulated-state error ϵ_j with I_{dc} values of 0 and 150 mA. (b) (i) Line cuts taken from panel a, showing the simulated ϵ_j as a function of u . (ii) Calculated Zeeman shift as a function of u for $I_{\text{dc}} = 150$ mA. (c) Measured transition frequency, with $I_{\text{dc}} = 150$ mA, for spins at different locations along a single diamond waveguide, as set by the optical excitation spot, exhibiting a position-dependent Zeeman shift. Error bars correspond to uncertainty in the location along the QMC. In the inset, a sample of ODMR measurements was used to determine the transition frequencies in the main plot. The spatially varying Zeeman shift allows for selective excitation of multiple spins. (d) Spins at different locations in the QMC are mapped to specific microwave frequency “addresses” for a given dc current. Experimentally measured frequency addresses are shown for multiple locations along three different diamond waveguides in our device (located between $u = 0$ and 14 μm). Waveguide 1 corresponds to the data shown in panel c.

dependent ω_j , yielding a Δ_j sufficiently large to satisfy the condition $\Omega_i/\Delta_j \ll 1$ even for closely spaced spins.

To demonstrate this experimentally, we apply a dc current ($I_{\text{dc}} = 150$ mA) to the microwave line. In ODMR measurements, the NV orientation corresponding to the 3 GHz feature at spot 2 (measured in Figure 2) shifts to 3.06 GHz, as one can see in the labeled measurement in Figure 3c. Mapping the transition frequency for this orientation subpopulation along the length of a single diamond waveguide (along coordinate u as shown in Figures 1a and 3a), the Zeeman shift increases to >160 MHz at $u = 2$ μm . This allows multiple spins in the same waveguide to be resolved, as shown in the inset. Here, the center of each ODMR dipole represents a π -rotation performed on spins at that particular location, thus demonstrating position-dependent selective control at multiple locations. Figure 3d summarizes the potential of this technique to enable the selective addressing of single spins within a dense register. The spatial variation of \vec{B}_{dc} allows each spin in the QMC to be mapped to a specific address, in either ω_{mw} or I_{dc} . Figure 3d shows the measured ω_{mw} address for spins at various locations within three waveguides of the QMC at an I_{dc} of 150 mA.

The NV electron spin is coupled to the nitrogen nuclear spin. For these simulations and measurements, we have considered the case in which manipulation of the electron spin is independent of the nuclear spin state. This leads to a trade-off between the control fidelity (improved by a larger Ω_i) and the reduction in ϵ_j (improved by a smaller Ω_j). For a discussion of the case in which there is no hyperfine coupling

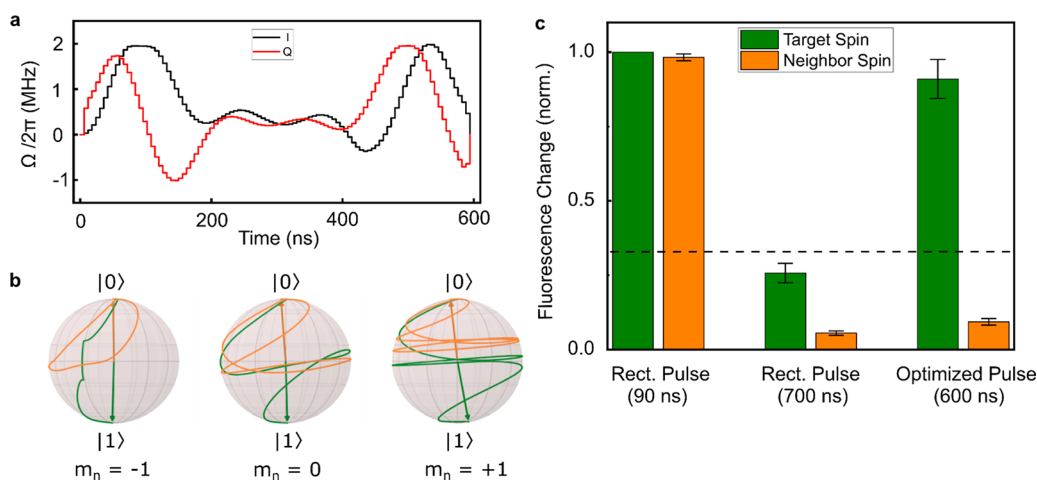


Figure 4. (a) Optimized pulse shape for selectively applying a π -rotation on spin i while leaving spin j unchanged, where $\omega_i - \omega_j = 1.1$ MHz. The amplitudes of the in-phase, \mathcal{I} (black), and out-of-phase, \mathcal{Q} (red), components of the microwave signal are shown as a function of time. (b) Calculated paths traced out on the Bloch sphere by spin i (green) and spin j (orange) during application of the optimized pulse. The hyperfine coupling to the nuclear spin has been included, and the spin evolution is shown for each of the three nuclear spin states, m_n . (c) Comparison of the cross-talk caused by rectangular control pulses and the optimized control pulse. The change in the spin-dependent fluorescence resulting from the application of the respective pulses is shown for each spin, normalized to the case of a rectangular pulse on resonance with that spin. The dashed line indicates the maximum expected fluorescence change ($1/3$) if the spin is flipped for only one hyperfine case. Error bars indicate the standard error of repeated measurements.

or the control is dependent on the nuclear spin, see [Supporting Information 6](#).

The scalability of this selective control scheme is limited by the steepness of the field gradient due to the requirement that $\Delta_j \gg \Omega_j$. Scaling to hundreds of spins and beyond calls for a technique for selectively controlling spins with more closely spaced transition frequencies. Using optimal control techniques, we can relax the requirement that $\Delta_j \gg \Omega_j$, pushing the limits of selective control even further.

Consider the special case of a spin flip operation performed on a single target spin i , and a single neighbor spin j that we wish to remain unchanged, with $\omega_i - \omega_j \neq 0$ and with both spins initialized into their respective ground states, $|0_i\rangle$ and $|0_j\rangle$. (See [Supporting Information 7](#) for examples of other control scenarios, including more than two spins and arbitrary rotations.)

Our optimal control technique works by shaping the time-dependent in-phase, $\mathcal{I}(t) = \frac{1}{2\pi}\Omega(t) \cos[\varphi(t)]$, and out-of-phase, $\mathcal{Q}(t) = \frac{1}{2\pi}\Omega(t) \sin[\varphi(t)]$, components of a microwave control pulse. This pulse is composed of m discrete time steps, with Ω and φ constants during each step. We then apply gradient descent^{36–40} to minimize a cost function, $f(\mathcal{I}, \mathcal{Q}) \equiv (1 - \varepsilon_i) + \varepsilon_j + R$, which includes the state error for each qubit, $\varepsilon_i = 1 - |\langle 0_i | \prod_{l=1}^m U_{i,l}(\mathcal{I}, \mathcal{Q}) | 0_i \rangle|^2$ and $\varepsilon_j = 1 - |\langle 0_j | \prod_{l=1}^m U_{j,l}(\mathcal{I}, \mathcal{Q}) | 0_j \rangle|^2$, where $U_{i,l}$ and $U_{j,l}$ are the evolution operators for a given time step l . Also included in the cost function is a regularization term, $R = \lambda \sum_{l=1}^{m-1} [|\mathcal{I}(t_l) - \mathcal{I}(t_{l+1})| + |\mathcal{Q}(t_l) - \mathcal{Q}(t_{l+1})|]$, weighted by λ (real, typically set to <1 MHz⁻¹), that is included to ensure that the pulse is smooth enough to be generated by the microwave source.

As mentioned above, the coupling between the NV electron spin and the nitrogen nuclear spin produces a hyperfine triplet with splitting at 2.2 MHz. The nuclear spin is in a mixed state, so to include this hyperfine interaction we model and average

over three two-level systems for both spin i and spin j . Optimally shaped pulses can be designed to flip one spin selectively on the corresponding nuclear spin state. However, experimentally, we consider the case in which manipulation of the electron spin is independent of the nuclear spin state. While this placed a limit on the effectiveness of frequency addressing, we show that our use of optimal control pulses can mitigate this limitation, as well.

We experimentally demonstrate an optimized control for the case in which $\Delta_j/2\pi = 1.1$ MHz. This represents an order of magnitude improvement in the minimum frequency separation needed for selective control compared to the $\Delta_j/2\pi > 20$ –30 MHz needed for the frequency resolution demonstrated in [Figure 3](#). [Figure 4a](#) shows the $\mathcal{I}(t)$ and $\mathcal{Q}(t)$ components of a control pulse designed using the optimization method described above. The calculated spin evolution during the application of this pulse is plotted in [Figure 4b](#) for each of the hyperfine states of i and j , with both spins starting at $|0\rangle$ and with an arrow indicating the end state.

We choose two spatially separated sites in the QMC and adjust I_{dc} to achieve $\Delta_j/2\pi = 1.1$ MHz for the two sites. For the purpose of demonstration, we selected two sites approximately 3 μm apart; however, as shown in [Figure 3c](#), this detuning can be realized for much more closely spaced spins. Spins at both sites are optically initialized into the $|0\rangle$ state. In [Figure 4c](#), we show, for each spin, the population found to be in the $|1\rangle$ state after the application of a microwave pulse, as measured by the change in fluorescence. This is normalized to the case of a rectangular π -pulse on resonance with that spin. A short, rectangular pulse can flip spin i with high fidelity; however, the cross-talk with spin j is significant ($\varepsilon_j > 0.9$). A longer rectangular pulse can achieve better resolution, but it becomes hyperfine-state selective, flipping at most a third of the population. In comparison, the optimized pulse successfully flips i while significantly reducing the level of cross-talk with j .

In our calculations, this pulse shape achieves an ε_j of 0.006 and an ε_i of 0.995; however, this is extremely sensitive to Δ_j ([Supporting Information 8](#)) as well as to pulse amplitude. The

higher level of cross-talk in our measurement is likely due to a limit in the precision with which these parameters were set, as well as to limitations in our spin-state measurements (see below).

We have demonstrated scalable methods for controlling spins in dense registers with a low level of cross-talk in a CMOS compatible PIC platform. Using an on-chip microwave signal line, we controlled the state of NV center spins hosted in optically integrated diamond waveguides. We also use this line to generate a local magnetic field gradient, enabling frequency addressing of multiple spins within a single waveguide for individual control. Finally, we use tailored microwave pulses optimized through a gradient-based search to selectively control spins where the requirement for frequency resolution is not met, demonstrating control with minimal cross-talk for frequency separations as small as 1.1 MHz.

These control methods can be applied to large numbers of spins (see Supporting Information 6), are fully coherent, and are compatible with state transfer to nuclear memories. While the measurements shown here are limited to π -rotations and state population readout, selective spin control is effective for arbitrary rotations. In this case, the criterion for frequency addressing ($\Omega_j/\Delta_j \ll 1$) remains the same (see Supporting Information 1), and the optimal control pulses can be designed to generate any desired end states (see Supporting Information 7).

To aid in optical integration and to explore the spatial dependence of the Zeeman shift, we used a diamond QMC with a moderately high density of color centers throughout (<1 ppm nitrogen concentration leading to >1 NV per excitation spot). This made spin-state measurements challenging due to a large position-dependent background from color centers of the wrong orientation and to the existence of multiple color centers of the correct orientation at different locations within the optical excitation spot. These limitations will be mitigated by using lower-density samples (<1 NV per excitation spot) and resonant optical addressing.^{6,32}

Our device used a single, straight line to generate the magnetic field gradient. In the future, more sophisticated line designs could allow for tailored gradient shapes and steepness, and multiple lines would enable tuning of the field direction for alignment with color centers.

The results shown here represent an important step toward the development of scalable quantum networks with nodes containing large numbers of spin qubits that can be selectively manipulated with high fidelity while being interfaced with on- and off-chip optics.

■ ASSOCIATED CONTENT

SI Supporting Information

The Supporting Information is available free of charge at <https://pubs.acs.org/doi/10.1021/acs.nanolett.3c01511>.

Derivation of the exact expression for the error function; layer stack and dimensions for the QMC and photonic chip; methods for microwave signal generation; additional ODMR, Rabi oscillation, and Zeeman shift measurements; simulations demonstrating the scalability of the selective control schemes; simulations demonstrating additional optimal control examples; and ODMR with the optimized pulse (PDF)

■ AUTHOR INFORMATION

Corresponding Authors

D. Andrew Golter – The MITRE Corporation, Bedford, Massachusetts 01730, United States; orcid.org/0000-0002-3443-6617; Email: dagolter@mitre.org

Genevieve Clark – The MITRE Corporation, Bedford, Massachusetts 01730, United States; Research Laboratory of Electronics, Massachusetts Institute of Technology, Cambridge, Massachusetts 02139, United States; Email: gclark@mitgre.org

Matt Eichenfield – Sandia National Laboratories, Albuquerque, New Mexico 87185, United States; College of Optical Sciences, University of Arizona, Tucson, Arizona 85719, United States; Email: eichenfield@arizona.edu

Gerald Gilbert – The MITRE Corporation, Princeton, New Jersey 08540, United States; Email: ggilbert@mitre.org

Dirk Englund – Research Laboratory of Electronics, Massachusetts Institute of Technology, Cambridge, Massachusetts 02139, United States; orcid.org/0000-0002-1043-3489; Email: englund@mit.edu

Authors

Tareq El Dandachi – Research Laboratory of Electronics, Massachusetts Institute of Technology, Cambridge, Massachusetts 02139, United States

Stefan Krastanov – Research Laboratory of Electronics, Massachusetts Institute of Technology, Cambridge, Massachusetts 02139, United States

Andrew J. Leenheer – Sandia National Laboratories, Albuquerque, New Mexico 87185, United States

Noel H. Wan – Research Laboratory of Electronics, Massachusetts Institute of Technology, Cambridge, Massachusetts 02139, United States

Hamza Raniwala – Research Laboratory of Electronics, Massachusetts Institute of Technology, Cambridge, Massachusetts 02139, United States

Matthew Zimmermann – The MITRE Corporation, Bedford, Massachusetts 01730, United States

Mark Dong – The MITRE Corporation, Bedford, Massachusetts 01730, United States; Research Laboratory of Electronics, Massachusetts Institute of Technology, Cambridge, Massachusetts 02139, United States; orcid.org/0000-0002-8577-451X

Kevin C. Chen – Research Laboratory of Electronics, Massachusetts Institute of Technology, Cambridge, Massachusetts 02139, United States

Linsen Li – Research Laboratory of Electronics, Massachusetts Institute of Technology, Cambridge, Massachusetts 02139, United States

Complete contact information is available at:

<https://pubs.acs.org/10.1021/acs.nanolett.3c01511>

Author Contributions

D.A.G. and G.C. contributed equally to this work. D.A.G. and G.C., with assistance from H.R., built the experimental setups and performed the experiments. T.E.D. and S.K. performed the gradient descent numerical analysis to design the microwave pulse shapes for optimal control, and M.Z. assisted in experimental microwave pulse generation. G.G. provided additional theory support. N.H.W., K.C.C., and L.L. designed and fabricated the diamond microchips. G.C. and N.H.W., with assistance from M.D., A.J.L., and M.E., designed the PIC for diamond integration. M.E. developed the PIC platform and

concept of operation. M.E. and A.J.L. developed the fabrication methodology of the PIC platform. D.E., D.A.G., and G.C. conceived the experiments. G.G., M.E., and D.E. supervised the project. D.A.G. and G.C. wrote the manuscript with input from all authors.

Notes

The authors declare no competing financial interest.

ACKNOWLEDGMENTS

Major funding for this work is provided by The MITRE Corp. for the Quantum Moonshot Program. N.H.W. acknowledges support from the Army Research Laboratory (ARL) Center for Distributed Quantum Information (CDQI) (Program W911NF-15-2-0067). H.R. acknowledges support from the NDSEG Fellowship and the NSF Center for Ultracold Atoms (CUA). K.C.C. acknowledges additional funding support by the National Science Foundation RAISE-TAQS (Grant 1839155). L.L. acknowledges funding from NSF QISE-NET Grant DMR-1747426 and the ARO MURI W911NF2110325. M.E. performed this work, in part, with funding from the Center for Integrated Nanotechnologies, an Office of Science User Facility operated for the U.S. Department of Energy Office of Science. D.E. acknowledges the National Science Foundation (NSF) Engineering Research Center for Quantum Networks (CQN), awarded under Cooperative Agreement 1941583.

REFERENCES

- (1) Choi, H.; Pant, M.; Guha, S.; Englund, D. Percolation-Based Architecture for Cluster State Creation Using Photon-Mediated Entanglement between Atomic Memories. *npj Quantum Information* **2019**, *5*, 104.
- (2) Nickerson, N. H.; Fitzsimons, J. F.; Benjamin, S. C. Freely Scalable Quantum Technologies Using Cells of 5-to-50 Qubits with Very Lossy and Noisy Photonic Links. *Phys. Rev. X* **2014**, *4*, No. 041041.
- (3) Nemoto, K.; Trupke, M.; Devitt, S. J.; Stephens, A. M.; Scharfenberger, B.; Buczak, K.; Nöbauer, T.; Everitt, M. S.; Schmiedmayer, J.; Munro, W. J. Photonic Architecture for Scalable Quantum Information Processing in Diamond. *Phys. Rev. X* **2014**, *4*, No. 031022.
- (4) Dong, M.; Clark, G.; Leenheer, A. J.; Zimmermann, M.; Dominguez, D.; Menssen, A. J.; Heim, D.; Gilbert, G.; Englund, D.; Eichenfield, M. High-Speed Programmable Photonic Circuits in a Cryogenically Compatible, Visible–near-Infrared 200 Mm CMOS Architecture. *Nat. Photonics* **2022**, *16*, 59.
- (5) Stanfield, P. R.; Leenheer, A. J.; Michael, C. P.; Sims, R.; Eichenfield, M. CMOS-Compatible, Piezo-Optomechanically Tunable Photonics for Visible Wavelengths and Cryogenic Temperatures. *Opt. Express* **2019**, *27*, 28588.
- (6) Wan, N. H.; et al. Large-Scale Integration of Artificial Atoms in Hybrid Photonic Circuits. *Nature* **2020**, *583*, 226.
- (7) Awschalom, D. D.; Hanson, R.; Wrachtrup, J.; Zhou, B. B. Quantum Technologies with Optically Interfaced Solid-State Spins. *Nat. Photonics* **2018**, *12*, 516.
- (8) Sukachev, D. D.; Sipahigil, A.; Nguyen, C. T.; Bhaskar, M. K.; Evans, R. E.; Jelezko, F.; Lukin, M. D. Silicon-Vacancy Spin Qubit in Diamond: A Quantum Memory Exceeding 10 Ms with Single-Shot State Readout. *Phys. Rev. Lett.* **2017**, *119*, No. 223602.
- (9) Maurer, P. C.; et al. Room-Temperature Quantum Bit Memory Exceeding One Second. *Science* **2012**, *336*, 1283.
- (10) Atatüre, M.; Englund, D.; Vamivakas, N.; Lee, S.-Y.; Wrachtrup, J. Material Platforms for Spin-Based Photonic Quantum Technologies. *Nature Reviews Materials* **2018**, *3*, 38.
- (11) Zhu, T.-X.; Liu, C.; Jin, M.; Su, M.-X.; Liu, Y.-P.; Li, W.-J.; Ye, Y.; Zhou, Z.-Q.; Li, C.-F.; Guo, G.-C. On-Demand Integrated Quantum Memory for Polarization Qubits. *Phys. Rev. Lett.* **2022**, *128*, No. 180501.
- (12) Chen, S.; Raha, M.; Phenicie, C. M.; Ourari, S.; Thompson, J. D. Parallel Single-Shot Measurement and Coherent Control of Solid-State Spins below the Diffraction Limit. *Science* **2020**, *370*, 592.
- (13) Sipahigil, A.; et al. An Integrated Diamond Nanophotonics Platform for Quantum-Optical Networks. *Science* **2016**, *354*, 847.
- (14) Bhaskar, M. K.; et al. Experimental Demonstration of Memory-Enhanced Quantum Communication. *Nature* **2020**, *580*, 60.
- (15) Schrunner, P. P. J.; Olthaus, J.; Reiter, D. E.; Schuck, C. Integration of Diamond-Based Quantum Emitters with Nanophotonic Circuits. *Nano Lett.* **2020**, *20*, 8170.
- (16) Patel, R. N.; Schröder, T.; Wan, N.; Li, L.; Mouradian, S. L.; Chen, E. H.; Englund, D. R. Efficient Photon Coupling from a Diamond Nitrogen Vacancy Center by Integration with Silica Fiber. *Light Sci. Appl.* **2016**, *5*, No. e16032.
- (17) Mouradian, S. L.; et al. Scalable Integration of Long-Lived Quantum Memories into a Photonic Circuit. *Phys. Rev. X* **2015**, *5*, No. 031009.
- (18) Nguyen, C. T.; et al. Quantum Network Nodes Based on Diamond Qubits with an Efficient Nanophotonic Interface. *Phys. Rev. Lett.* **2019**, *123*, No. 183602.
- (19) Awschalom, D. D.; Bassett, L. C.; Dzurak, A. S.; Hu, E. L.; Petta, J. R. Quantum Spintronics: Engineering and Manipulating Atom-like Spins in Semiconductors. *Science* **2013**, *339*, 1174.
- (20) Pingault, B.; Jarausch, D.-D.; Hepp, C.; Klintberg, L.; Becker, J. N.; Markham, M.; Becher, C.; Atatüre, M. Coherent Control of the Silicon-Vacancy Spin in Diamond. *Nat. Commun.* **2017**, *8*, 15579.
- (21) Hensen, B.; et al. Loophole-Free Bell Inequality Violation Using Electron Spins Separated by 1.3 Kilometres. *Nature* **2015**, *526*, 682.
- (22) Humphreys, P. C.; Kalb, N.; Morits, J. P. J.; Schouten, R. N.; Vermeulen, R. F. L.; Twitchen, D. J.; Markham, M.; Hanson, R. Deterministic Delivery of Remote Entanglement on a Quantum Network. *Nature* **2018**, *558*, 268.
- (23) Pompili, M.; et al. Realization of a Multinode Quantum Network of Remote Solid-State Qubits. *Science* **2021**, *372*, 259.
- (24) Bernien, H.; et al. Heralded Entanglement between Solid-State Qubits Separated by Three Metres. *Nature* **2013**, *497*, 86.
- (25) Metsch, M. H.; Senkalla, K.; Tratzmiller, B.; Scheuer, J.; Kern, M.; Achard, J.; Tallaire, A.; Plenio, M. B.; Siyushev, P.; Jelezko, F. Initialization and Readout of Nuclear Spins via a Negatively Charged Silicon-Vacancy Center in Diamond. *Phys. Rev. Lett.* **2019**, *122*, No. 190503.
- (26) Bartling, H. P.; Abobeih, M. H.; Pingault, B.; Degen, M. J.; Loenen, S. J. H.; Bradley, C. E.; Randall, J.; Markham, M.; Twitchen, D. J.; Taminiau, T. H. Entanglement of Spin-Pair Qubits with Intrinsic Dephasing Times Exceeding a Minute. *Phys. Rev. X* **2022**, *12*, No. 011048.
- (27) Bradley, C. E.; Randall, J.; Abobeih, M. H.; Berrevoets, R. C.; Degen, M. J.; Bakker, M. A.; Markham, M.; Twitchen, D. J.; Taminiau, T. H. A Ten-Qubit Solid-State Spin Register with Quantum Memory up to One Minute. *Phys. Rev. X* **2019**, *9*, No. 031045.
- (28) Dutt, M. V. G.; Childress, L.; Jiang, L.; Togan, E.; Maze, J.; Jelezko, F.; Zibrov, A. S.; Hemmer, P. R.; Lukin, M. D. Quantum Register Based on Individual Electronic and Nuclear Spin Qubits in Diamond. *Science* **2007**, *316*, 1312.
- (29) Neumann, P.; Beck, J.; Steiner, M.; Rempp, F.; Fedder, H.; Hemmer, P. R.; Wrachtrup, J.; Jelezko, F. Single-Shot Readout of a Single Nuclear Spin. *Science* **2010**, *329*, 542.
- (30) Dong, M.; et al. Piezo-Optomechanical Cantilever Modulators for VLSI Visible Photonics. *APL Photonics* **2022**, *7*, No. 051304.
- (31) Dong, M.; et al. Programmable Photonic Integrated Meshes for Modular Generation of Optical Entanglement Links. *npj Quantum Information* **2023**, *9*, 42.
- (32) Bersin, E.; Walsh, M.; Mouradian, S. L.; Trusheim, M. E.; Schröder, T.; Englund, D. Individual Control and Readout of Qubits in a Sub-Diffraction Volume. *npj Quantum Information* **2019**, *5*, 38.

- (33) Grinolds, M. S.; Maletinsky, P.; Hong, S.; Lukin, M. D.; Walsworth, R. L.; Yacoby, A. *Quantum Control of Proximal Spins Using Nanoscale Magnetic Resonance Imaging*. *Nat. Phys.* **2011**, *7*, 687.
- (34) Zhang, H.; Arai, K.; Belthangady, C.; Jaskula, J.-C.; Walsworth, R. L. Selective Addressing of Solid-State Spins at the Nanoscale via Magnetic Resonance Frequency Encoding. *npj Quantum Information* **2017**, *3*, 31.
- (35) Sekiguchi, Y.; Matsushita, K.; Kawasaki, Y.; Kosaka, H. Optically Addressable Universal Holonomic Quantum Gates on Diamond Spins. *Nat. Photonics* **2022**, *16*, 662.
- (36) Khaneja, N.; Reiss, T.; Kehlet, C.; Schulte-Herbrüggen, T.; Glaser, S. J. Optimal Control of Coupled Spin Dynamics: Design of NMR Pulse Sequences by Gradient Ascent Algorithms. *J. Magn. Reson.* **2005**, *172*, 296.
- (37) Heeres, R. W.; Reinhold, P.; Ofek, N.; Frunzio, L.; Jiang, L.; Devoret, M. H.; Schoelkopf, R. J. Implementing a Universal Gate Set on a Logical Qubit Encoded in an Oscillator. *Nat. Commun.* **2017**, *8*, 94.
- (38) Rembold, P.; Oshnik, N.; Müller, M. M.; Montangero, S.; Calarco, T.; Neu, E. Introduction to Quantum Optimal Control for Quantum Sensing with Nitrogen-Vacancy Centers in Diamond. *AVS Quantum Sci.* **2020**, *2*, 024701.
- (39) Nöbauer, T.; Angerer, A.; Bartels, B.; Trupke, M.; Rotter, S.; Schmiedmayer, J.; Mintert, F.; Majer, J. Smooth Optimal Quantum Control for Robust Solid-State Spin Magnetometry. *Phys. Rev. Lett.* **2015**, *115*, No. 190801.
- (40) Krastanov, S.; Zhou, S.; Flammia, S. T.; Jiang, L. Stochastic Estimation of Dynamical Variables. *Quantum Sci. Technol.* **2019**, *4*, No. 035003.